2D-Image analysis: A complementary tool for characterizing quarry and weathered building limestones.

Olivier Rozenbaum, Emmanuel Le Trong, Jean-Louis Rouet, Ary Bruand

2D-Image analysis: A complementary tool for characterizing quarry and weathered building limestones.

Olivier ROZENBAUM*, Emmanuel LE TRONG, Jean-Louis ROUET, Ary BRUAND

Olivier. ROZENBAUM*,
Assistant professor,
Institut des Sciences de la Terre d'Orléans (ISTO)
UMR6113 CNRS/Université d'Orléans
1A, rue de la Férollerie
45071 Orléans Cedex 2
rozenbaum@cnrs-orleans.fr
Phone: 332-38-25-52-44
Fax: 332-38-63-64-88
*Corresponding author

Emmanuel LE TRONG,
Post-doctorant,
Institut des Sciences de la Terre d'Orléans (ISTO)
UMR6113 CNRS/Université d'Orléans
1A, rue de la Férollerie
45071 Orléans Cedex 2
manu@mixtion.org
Phone: 332-38-25-53-99
Fax: 332-38-63-64-88

Jean-Louis ROUET,
Professor,
Institut des Sciences de la Terre d'Orléans (ISTO)
UMR6113 CNRS/Université d'Orléans
1A, rue de la Férollerie
45071 Orléans Cedex 2
Jean-Louis.Rouet@labomath.univ-orleans.fr
Phone: 332-38-25-57-27
Fax: 332-38-63-64-88

Ary BRUAND
Professor,
Institut des Sciences de la Terre d'Orléans (ISTO)
UMR6113 CNRS/Université d'Orléans
1A, rue de la Férollerie
45071 Orléans Cedex 2
Ary.Bruand@univ-orleans.fr
Phone: 332-38-25-53-98
Fax: 332-38-63-64-88

Running head

2D-Image analysis of quarried and weathered limestones

Abstract

Understanding of weathered processes and more generally of transfer properties of building stone requires a detailed knowledge of the porosity characteristics. This study aims at analyzing 2D-images of stones by using mathematical tools that enable the description of the pore and solid phase distribution. We selected two limestones that were widely used for different types of buildings: a quarried and weathered tuffeau, the latter being used in most Châteaux of the Loire and a quarried sebastopol stone used in numerous buildings in Paris. Backscattered electron scanning images obtained on thin section of the stones were studied by using autocorrelation function analysis and chord distributions. Our results showed that these mathematical tools are able to discuss quantitatively and statistically differences of pore and solid distribution between quarried limestones, and to discuss the weathering degree of stones collected on buildings. Thus, very small differences of pore and solid phase distribution between the samples studied were revealed by chord distribution analysis and autocorrelation function analysis. The resulting characteristics obtained with such an analysis are promising information for a better understanding of the weathering mechanisms.

Key word

Image analysis, limestones, building, quarry, weathering, porosity, chord length distribution, autocorrelation function.

1. Research aims

The external environmental agents, such as rain, wind, temperature and pollution are the main factors of stone weathering [1-3]. Pollutants such as particulate matter originating from industry and vehicle exhaust (combustion of oil-derived fuels) and SO_2 combined with wetting/drying cycles are responsible for the alteration by sulfating building limestones [3-7]. Indeed, the acid attack of these geomaterials leads to the dissolution of carbonates and the formation of sulfate compounds (mainly gypsum). The result is a radical change in the porous and solid phase characteristics of the stone in depth (from a few micrometers down to a few centimeters depth), leading to its irreparable destruction. The depth and the weathering facies depend both on the environment factors and the stone characteristics [2]. Besides, a good understanding of the weathering mechanisms requires to relate the microstructure characteristics to the macroscopic properties (permeability, friability, etc.). Thus, it is important to characterize stones originating from carriers and weathered buildings as an initial step for other studies in the field of building stone conservation.

As water transfer and mechanical properties are linked to the porous network characteristics, our objective is the morphological and structural characterization of the stones. So, how to characterize a disordered porous medium such as those of stones? Some classical experiments are commonly used to characterize the porous phase such as mercury intrusion porosimetry (e.g. [8-9]), nitrogen BET (e.g. [10]) or image analysis (e.g. [11-12]). It should be kept in mind that the two first techniques measure a pore throat size distribution

depending on the cross-sectional throat shape and topology of the pore throat network. Theses techniques give in first approximation an equivalent circular cross sectional diameter by the way of a geometrical model giving inaccurate information on the pore size, even if they produce a good first approach of the porous lattice. In this study we present others tools that are based on image analysis and that enable to improve our knowledge of the solid and porous phase distribution in a stone. Indeed, image analysis provides a huge quantity of data, important to complement the characterization of the porous medium as explained in the last part of this paper. The present work focuses on computerized 2D image analysis using mathematical tools characterizing geomaterials in different ways. Within the last twenty years, analysis of images produced by using optical microscopy or scanning electron microscopy (SEM) were commonly used to characterize different porous materials such as porous silica, soils, concrete, stones etc [13-14].

In this paper, we selected two quarry limestones used as building stones and a weathered limestone originating from a church. Our aim is the quantitative characterization of the pore and solid phases of the stone by using mathematical tools applied to image analysis. The present samples were selected because they have been widely studied earlier by classical techniques [15-17]. Nevertheless the mathematical tools presented here can be used for other stones and purposes.

2. Material and method.

2.1. Materials

In order to show how 2D computerized image analysis of the pore and solid phase distribution can be used in monument conservation, quarry and weathered limestones were selected. Two non weathered limestones were selected: a tuffeau and a sebastopol stone.

The tuffeau was collected in a quarry located nearby the village of Saint-Cyr-en-Bourg (France). Historically, the tuffeau was chosen to build most Loire chateaux, churches, cathedrals, and houses along the Loire valley. This stone is an easily workable building material. Today, the tuffeau is mainly used for the restoration of these buildings. Tuffeau is a yellowish-white porous sedimentary limestone and mainly characterized in the last decade [15-17]. This is a siliceous limestone of Middle Turonian age (90 10^6 yrs) located principally between the cities of Angers and Tours along the Loire and the Vienne rivers. Previous studies [16-17] showed that the tuffeau is essentially composed of calcite, silica in the form of opal cristobalite-tridymite and quartz and some secondary minerals such as clays and micas. The tuffeau used was composed of 50.3 % of calcite and 45.2 % of silica (determined by induced chemical plasma) and the total porosity obtained by density measurement was 48.1 %. It is a multiscale porous medium since the equivalent pore size distribution ranged from 0.01 to 50 μm in size [18].

The sebastopol stone was collected in a quarry located in the North of Paris. This stone is a yellowish-beige sedimentary limestone composed essentially of calcite and quartz. It was formed during the middle Lutetian (45 10^6 yrs). It was used to build historic buildings in Paris. The sebastopol stone used was mainly composed of 81.6 % of calcite and 16.8 % of silica (determined by induced chemical plasma). The total porosity was 43.4 % but with a pore size distribution corresponding to bigger pores than those forming the porosity of the tuffeau.

Indeed, the equivalent pore size distribution ranged from 0.5 to 200 µm in size [18].

A weathered tuffeau was also selected. It originated from the Saint-Donatien church located in Orléans (France). The blocks were extracted from the north-east wall of the bell tower at an elevation of 20 meters. Sampling occurred during the restoration of the church that consisted in the whole replacement of the block by news ones. The exposed surface was a grey crust harder than the stone core and the first three centimeters underneath that surface was crumbly with micro-cracks parallel to the surface. A block was selected and, as the weathering degree decreased with depth from the surface, the stone was sampled in the 0-55 mm range from the surface. Chemical analyses (induced chemical plasma and infrared spectroscopy) confirm that this stone is mainly composed of calcite and silica as the quarry tuffeau [16-17]. Infrared spectroscopy and microprobe analysis showed that gypsum is present in the first 30 mm from the surface but essentially concentrated in the first 20 µm, corresponding to the grey crust [19].

2.2. Obtaining the 2D images

We acquired 2D images for quantitative analysis by using scanning electron microscopy on thin sections (30×45 mm^2). The latter were obtained after sample impregnation with a polyester resin under vacuum. The thin sections were polished and coated with carbon prior to observation using the backscattered electron emission [20]. Thin sections parallel to the stone bed were produced for the quarry stones. For the weathered tuffeau, two thin sections were produced perpendicular to the exposed surface, one enabling the study from the surface to

25 mm depth and the other one, from 25 to 50 mm depth. We recorded Backscattered Electron Scanning Images (BESI) consisting of arrays of 736×500 pixels for quarry tuffeau samples (736×400 for weathered tuffeau) and 1024×800 pixels for sebastopol stone samples, each pixel having 8 bits depth (256 grey scales). The resolution was 2.8 and 3.8 µm per pixel for the tuffeau and sebastopol stones samples, respectively.

2.3. Image analysis and segmentation

One of the main problems in image analysis of porous materials lies in the distinctions between the pore and the solid phase. This is mainly related to the finite pixel size, noise caused by data acquisition or inappropriate sample preparation. For geometrical analysis of 2D images, it is required to use a well defined method permitting to determine whether a pixel belongs to the pore or to the solid phase. This procedure is known as image segmentation and must be reliable and accurate. Segmentation is the process that consists in converting a grey-scale image into a binary image by identifying two sets of pixels in the image on the basis of their grey level. Usually the threshold value is chosen accordingly to the shape of the grey level histogram. This procedure leads to good results if the histograms of the two phases are clearly separated. Homemade algorithms were implemented in C++ in order to calculate the histograms, to determine the thresholds and to segment the images. Twenty nine images were analysed: 8 and 7 images for respectively the tuffeau and the sebastopol stone originating from a quarry, and 14 images for the weathered tuffeau.

3. Results and discussion

3.1. Pore and solid phase morphology

Scanning electron microscopy realized on fracture at high resolution (not shown here) and the BESI (*Figure 1a and b*) showed that the sebastopol limestone was composed of bigger grains (mainly 1 to 400 µm in size) than the quarry tuffeau (mainly 0.1 to 150 µm) thus resulting in greater pores in the sebastopol stone. Furthermore, the grains of the sebastopol stone appear to be less cemented than those of the tuffeau. For the weathered tuffeau originating from the church three zones are distinguished according to both weathering intensity and depth. The BESI showed a strongly weathered zone from the surface to 2 mm depth (*Figures 1c and d*) with the presence of large pores, some of them being elongated pores corresponding to cracks. The BESI showed also deeper a moderately weathered zone from 2 mm to 30 mm depth (*Figure 1e*) where cracks are still present even if the pores are smaller than in the strongly weathered zone. Then, deeper there is no crack, the tuffeau looks unaltered and similar to the quarry tuffeau (*Figure 1f*).

The grey level histograms recorded for the images studied were bimodal (*Figure 2*). Most pore phase corresponded to the [0-65] grey level range and most solid phase to the [65-255] grey level range. The threshold value was taken as equalled to 65, i.e. at the minimum between the two distributions. Our results showed also that a little change of grey level (± 5) for this threshold value does not impinge strong modifications in the segmented resulting image (*Figure 3*).

3.2. Porosity

Measurement of porosity on a 2D image requires measurements on a representative elementary surface area (RESA). A RESA is a surface area over which a statistical averaged property can be computed. The RESA should be extracted from a large enough image size to provide representation of the macroscopic properties of the media. The RESA is not always caught by the experimental images acquisition and must be estimated for every new image. The determination of the RESA is implemented by taking a small surface area within an image and by calculating the property of interest (e.g. porosity). The small surface area is then expanded in all directions and the property recalculated. The RESA is determined as the surface area value over which the property of interest remains constant.

Classically total porosity (ϕ) is defined as following:

$$\phi = \frac{V_p}{V_p + V_s}, \qquad (1)$$

where V_p and V_s, are the volume of the pore and solid phase, respectively. For a 2D digitized medium, V_p and V_s are the number of pixels corresponding to the porous phase and to the solid phase, respectively.

In order to estimate the RESA of ϕ, the porosity was measured for different image size and three examples are given in *Figure 4*. As expected for the smallest area, the porosity varies extremely but, as the image size increases, the porosity tends to a limit. Obviously, this limit represents the porosity for pores larger than the pixel size resolution. It can be concluded that the RESA exists for

the samples studied and is reached for the whole image (at least for total porosity). Results showed that the RESA corresponded to a surface area of about 2.10^5 pixels squares for these resolutions. This surface area corresponded to 1.6 and 2.9 mm^2 for the tuffeau and sebastopol stone respectively.

In table 1 are reported the average porosities calculated for the different stones. The standard deviations are similar for the stones studied and are relatively small. The porosity of the sebastopol stone is slightly higher than the one of the quarry tuffeau. The porosity determined by image analysis for the tuffeau originating from the quarry (30.5 %) is much smaller than the porosity determined from density measurement (48.1 %) [18]. That difference is related to the small pores that are not taken into account in image analysis because they are smaller than the resolution (2.8 µm). This behaviour is also encountered with the sebastopol stone which has porosity determined by image analysis of 35.6 % (3.8 µm pixel size resolution) and a porosity determined from density measurement of 43.4 % [18].

3.3. Autocorrelation function

The autocorrelation function is another tool enabling the statistical description of porous medium. In the following we define the two point correlation function, keeping in mind that a correct description of correlations is done by calculating the n-point correlation functions [21]. Let $\vec{x}$ the position vector from an arbitrary origin and $\Psi_m(\vec{x})$ being a density function defined as: $\Psi_m(\vec{x}) = 1$ if $\vec{x}$ belongs to the pore space and $\Psi_m(\vec{x}) = 0$ if $\vec{x}$ belongs to the solid

space. The porosity ϕ and the two point correlation function $S_2(\vec{r})$ can be defined by the statistical averages [22-23]:

$$\phi = < \Psi_m(\vec{x}) > \quad (2)$$

$$S_2(\vec{r}) = < \Psi_m(\vec{x})\Psi_m(\vec{r}+\vec{x}) > . \quad (3)$$

The brackets <> means surface average over the spatial coordinates $\vec{x}$. Writing the last equation in this way assumes that the porous medium is statistically homogeneous. In other words, on average, only differences between two coordinate values are important and not their absolute location. The two limits of $S_2(\vec{r})$ are [24]:

$$S_2(0) = \phi \quad (4)$$

$$\lim_{r\to\infty} S_2(\vec{r}) = \phi^2 \quad (5)$$

With these limits, the autocorrelation function $R_Z(\vec{r})$ can be defined in order to have a normalized function:

$$R_Z(\vec{r}) = \frac{< (\Psi_m(\vec{x}) - \phi).(\Psi_m(\vec{r}+\vec{x}) - \phi) >}{\phi(1-\phi)} . \quad (6)$$

This function can be interpreted as the probability of finding two randomly selected points that are both in the same phase. For an isotropic medium with $r = |\vec{r}|$, $R_Z(\vec{r}) = R_Z(r)$, the autocorrelation function is a function of distance only. Otherwise, the one dimension autocorrelation functions for $\vec{r}$ parallel to the Ox or Oy axis, respectively noted R_{Zx}, R_{Zy} give information about isotropy or anisotropy. Indeed, pore space anisotropy is revealed as a disparity between the one-dimensional autocorrelation functions along different directions [25]. However, the autocorrelation function does not provide information about the connectedness of the phases.

We calculated the autocorrelation functions R_{Zx}, R_{Zy} and the average value R_Z for the different samples. An example of the recorded autocorrelation function is given in *Figure 5*. All these functions present a decreasing behaviour without any particular correlation. Besides, a little disparity depending on the images was observed for the one dimensional autocorrelation functions along the orthogonal x and y-directions. The tuffeau (*Figure 5a*) and sebastopol stone (not shown here) originating from the quarry present both no or very slight anisotropies. The anisotropy is greater in the apparently moderately (*Figure 5a*) and the strongly (not shown here) weathered zone of the weathered tuffeau. This can be related to the presence of cracks or to a preferential dissolution of the solid phase that is not isotropic since it develops from the surface. Finally, comparison of the autocorrelation functions recorded for the quarry tuffeau and sebastopol stone confirmed that the characteristic dimensions of the sebastopol stone are higher than those of the tuffeau (*Figure 6*).

3.4. Chord distributions

Chord distributions are stereological tools allowing the description of the interface between pore and solid phase. A chord is a segment belonging either to the pore or to the solid phase and having both ends on the interface (*Figure 7*). The chord distribution gives the probability to have a chord length between r and r+dr. The chord distribution can be calculated either for the pores ($f_p(r)$ is called the pore chord distribution) and for the solid ($f_s(r)$ is called the solid chord distribution). The chords are calculated along randomly distributed lines in the

porous medium. Furthermore, the first momentum of $f_p(r)$ (called l_p) and the first momentum of $f_s(r)$ (called l_s) are defined as:

$$l_p(r) = \int r\, f_p(r)\, dr \qquad (6)$$

and,

$$l_s(r) = \int r\, f_s(r)\, dr\,. \qquad (7)$$

The values of l_p and l_s can be discussed as estimators of the mean size of the pore and solid phase.

Results showed that the greater was the chord length, the noisier was the chord distribution recorded (*Figure 8*). This noise corresponds to the large phases (pore or solid) that are very few in an image of finite size. Due to digitizing the smallest pores are badly defined and do not correspond to real objects. So, for r<3 pixels, chord distributions present a linear increase that has no reality and have not to be taken into account [14]. Most pore and solid chord distributions studied present an exponential decrease in a large range of chord length. The mathematical expressions of these distributions are [13]:

$$f_p(r) \equiv \exp(-r/\alpha_p) \qquad (8)$$

and

$$f_s(r) \equiv \exp(-r/\alpha_s) \qquad (9)$$

where α_p is the persistence length for the porous phase and α_s is the persistence length for the solid phase. These two persistence lengths α_p and α_s correspond to the mean distance between two interfaces across the pore and the solid phase respectively. Cousin *et. al.* [14] suggested to use an image size superior to four times the persistence lengths to study the chord distributions with a representative surface area. This type of porous media, in which both the porous and solid chord

distributions are exponential, is called a long-range random medium [13]. In other words, the pore and solid phase in the image are randomly distributed. The absence of correlation peaks demonstrate that the pore and solid phase are heterogeneously distributed in size. In the case of such exponential decay, $\alpha_p = l_p$ and $\alpha_s = l_s$.

The pore and solid chord distributions of the quarry tuffeau and sepastopol stones were calculated for different images taken in the same thin sections for each type of stone. The distributions present an exponential decay (*Figure 8 and Figure 9*) but within a larger chord length range for the sebastopol stone. Differences between the pore chords distributions for both stones were recorded for the longest chords, related to the presence of large pores in the images. The solid chord distributions show also an exponential decay except for the longest chords because of the presence of some large grains. The first moments of the chord distributions are in average for the tuffeau $l_p \approx 10$ µm and $l_s \approx 22$ µm and for the sebastopol stone $l_p \approx 26$ µm and $l_s \approx 47$ µm. Thus, even if the total porosities are equivalent, the pore and solid phases of the sebastopol stone is 2 or 3 times greater than those of the tuffeau as shown in *Figure 10*. The little variations in the whole range of the chord length show an important point: the chord distributions are able to capture little differences between different images. Theses deviations are due to the natural heterogeneity of geomaterials. Nevertheless, the chord distributions present the same behaviour and are representative of the stone. Thus, the chord distributions are very sensitive to some geometrical fluctuations, then making possible to reveal small heterogeneities in geomaterials.

The solid chord distributions enable the distinction of the strongly weathered zone from the moderately or no weathered zone. Indeed, results

showed that $l_s \approx 14$ µm for the former and $l_s \approx 23$ µm for the later (*Figure 11*). These solid chord distributions form two sets easily distinguishable: the solid chord distributions of the strongly weathered zone have always higher persistence length (shown by the slopes in the semi logarithmic representation) than the solid chord distributions of the moderately or no weathered zone. Thus, the distance between two interfaces within the solid phase is statistically greater in the moderately or no weathered zone than in the strongly weathered zone. This distinction would result from dissolution processes resulting in bigger pores in the strongly weathered zone. The existence of the cracks does not change the solid chord distributions but affects the pore chord distributions in the range of the longest chords. Indeed, the pore chord distribution of the moderately weathered zone (*Figure 11a*) where cracks are present has a higher slope than the pore chord distribution of the no weathered zone (*Figure 11b*) for chords >100 µm but are similar for smaller chord. Up to 100 µm, the pore chord distribution of the moderately weathered zone (*Figure 11a*) can be described by a second exponential function representative of the cracks. This is exactly the same remark for the pore chord distributions of both strongly weathered zones studied (*Figure 11c and d*). The pore chord distributions of the moderately or no weathered zone and of a strongly weathered zone (respectively *Figure 11a*, *b*, and *d*) are similar for the chords <100 µm, but for another strongly weathered zone (*Figure 11c*), the pore chord distribution has a lower slope than the others showing that the distance between two interfaces within the pore phase in this image is always statistically greater. This behaviour was expected for the moderately or no weathered zone in comparison with the strongly weathered zone (*Figure 1 c and 11c*). But, this can be surprising for the comparison between the two pore chord distributions of the

strongly weathered zones. In fact, as the solid chord distributions of the two strongly weathered zones studied are similar (proving the same “rate” of dissolutions), it can be assumed that the presence of larges cracks (*Figure 1c*) indicates a deep modification of the porosity, even in the range of the smallest pores (*Figure 11c*). This is not the case for the pore chord distributions of the moderately weathered zone. Thus, the thin cracks shown in the moderately weathered zone would indicate few modifications for the inter-grain pores of the tuffeau.

Furthermore, the ratio ls/lp might be also an interesting criterion for the study of the effect of weathering on stones. With the images of the no weathered zone, this ratio was in average 2.4 when it was 1.2 with images of strongly weathered zone. This result is quite intuitive because the mean size of the solid phase decreases (and the mean size of the porous phase increases) due to weathering consequences.

3. Conclusion

Our results showed that the mathematical tools presented in this paper are able to reveal quantitatively and statistically differences between quarried limestones. They showed also that they are able to distinguish clearly the weathering degree of stones collected on buildings. The resulting characteristics are promising information for a better understanding of the weathering mechanisms.

The chord distribution enables the study of the pore and solid phase repartition whatever the total porosity and thus enables to show very small

differences in pore morphology and pore structure between quarry stones or different zones of a weathered stone.

The autocorrelation function analysis showed that the quarried stones appeared as being an isotropic porous geomaterial at the study scale and when the 2-images studied are parallel to the stone bed. Discussion of the isotropy in the direction perpendicular to the stone bed will requires 2-D images taken parallel to that perpendicular direction. However, the discussion of the porosity characteristics with the aim to understand better the weathering mechanisms and more generally the transfer properties of the stone studied, requires 3-D analysis of the porosity characteristics. The mathematical tools applied to 2-D images in this study can be easily extended to 3-D images. This will be the next step by using 3-D images obtained by X-ray microtomography with the same stone samples.

References

[1] Camuffo D., Physical weathering of stones, Sci. Total Environ., 1995, 167, 1-14.

[2] Torok A. Oolitic limestone in a polluted atmospheric environment in Budapest: weathering phenomena and alterations in physical properties, from Natural stone, weathering phenomena, conservation strategies and case studies, Geological society of London, 2002, 205, 363-379.

[3] Lefèvre R.A. , Ausset P., Atmospheric pollution and building materials: stone and glass, Geological Society, Special Publication " Natural Stone, Weathering Phenomena, Conservation Strategies and Case Studies ", London, 2002, 205, 329-345.

[4] Monforti F., Bellasio R., Bianconi R., Clai G., Zanini G., An evaluation of particle deposition fluxes to cultural heritage sites in Florence, Italy, Sci. Total Environ., 2004, 334– 335, 61–72.

[5] Dolske D.A., Deposition of atmospheric pollutants to monuments, statues, and buildings, Sci. Total Environ., 1995, 167, 15-31.

[6] Hamilton R.S., Revitt D.M., Vincent K.J., Butlin R.N., Sulphur and nitrogen particulate pollutant deposition on to building surfaces, Sci. Total Environ., 1995, 167, 57-66.

[7] Rodriguez-Navarro C., Sebastian E. Role of particulate matter from vehicle exhaust on porous building stones (limestone) sulfation Sci. Total Environ., 1996, 187, 79-91.

[8] Bruand A., Prost R. Effect of water content on the fabric of a soil material: an experimental approach. J Soil Sci., 38, 1987, 461-472.

[9] Renault P., Theoretical Studies of Mercury Intrusion in Some Networks: Testing the Applicability of Mercury Intrusion in the Size Characterisation of the Lacunar Pore Space of Soil Samples", Trans. Porous Media, **3**, 1988, 529-547.

[10] Brunauer S., Emmett P.H., Teller E., Adsorption of gases in multimolecular layers, J. Am. Chem. Soc. 60, 1938, 309-324.

[11] Torok A., Rozgonyi N, Morphology and mineralogy of weathering crusts on highly porous oolitic limestone, a case study from Budapest, Environ. geol., 46, 2004, 333-349.

[12] D'Acqui L.P., Bruand A., Pagliai M., Study of soil porosity with mercury porosimetry and image analysis on backscattered electron scanning images (BESI). Application to tilled "crusting soils" in Zimbabwe. Soil micromorphology: studies in management and genesis. Proceedings of the IX International Working Meeting on Soil Micromorphology, Townsville, Australia, July 1992. Developments in soil science 22, 581-590.

[13] Levitz P., Tchoubar D., Disordered porous solids: from chord distribution to small angle scattering, J. Phys I, 1992, 2, 771-790.

[14] Cousin I., Levitz P., Bruand A., Three-dimensional analysis of a loamy-clay soil using pore and solid chord distributions, Europ. J. Soil Sci., 1996, 47, 439-452.

[15] Beck K., Al-Mukhtar M., Rozenbaum O., Rautureau M., Characterization, water transfer properties and deterioration in tuffeau: building material in the Loire valley, France, Building and Environ., 38, 2003, 1151-1162.

[16] Dessandier D., Etude du milieu poreux et des propriétés de transfert des fluides du tuffeau blanc de Touraine. Application à la durabilité des pierres en œuvre, Ph-D-Thesis, University of Tours, France, 1995.

[17] Brunet-Imbault B., Etude des patines de pierres calcaires mises en oeuvre en région Centre, Ph-D-Thesis, University of Orléans, France, 1999.

[18] Arrizi A., Personal communication, 2005.

[19] Anne S., Analyse de l'altération d'un tuffeau mis en œuvre, Master of Science and Technology, University of Orléans, France, 2005.

[20] Bruand A., Duval O., Calcified fungal filaments in the petrocalcic horizon of Eutrochrepts in Beauce (France). SSSAJ, 63, 1999, 164-169.

[21] Torquato S., Random heterogeneous materials, Springer 2002.

[22] Berryman, J.G., Measurement of spatial correlation functions using image processing techniques, J. Appl. Phys., 57(7), 1985, 2374–2384.

[23] Berryman J.G., Blair S.C., Use of digital image analysis to estimate fluid permeability of porous materials: Application of two-point correlation functions, J. Appl. Phys, 60 (6), 1986, 1930-1938.

[24] Coker D.A., Torquato S., Extraction of morphological quantities from a digitized medium, J. Appl. Phys. 77 (12), 1995.

[25] Frykman P., Rogon T.A., Anisotropy in pore networks analyzed with 2-D autocorrelation (variomaps), Computers and Geosciences, 1993, 19, 887-930.

Figures captions

Figure 1: Backscattered electron scanning images of (a) a quarried tuffeau, (b) a quarried sebastopol stone,(c) and (d) the strongly weathered zone, (e) moderately weathered zone of a weathered tuffeau and (f) the no weathered zone of a weathered tuffeau.

Figure 2: Grey level histogram recorded for the image of tuffeau shown in Figure 1e.

Figure 3: (a)Backscattered electron scanning image of a quarried tuffeau and (b) the same image after segmentation.

Figure 4: Total porosity versus the surface area of the image of (a) a quarried tuffeau, (b) a quarried sebastopol stone, (c) the strongly weathered zone of a weathered tuffeau.

Figure 5: Autocorrelation functions recorded for (a) a quarried tuffeau, (b) and the moderately weathered zone of a weathered tuffeau.

Figure 6: Autocorrelation functions of the quarried tuffeau and sebastopol limestone.

Figure 7: Schematic illustration of the pore chord distribution (pore phase in white and solid phase in grey).

Figure 8: Pore and solid chord distribution recorded for different images of a quarried tuffeau.

Figure 9: Pore and solid chord distribution recorded for different images of a quarried sebastopol stone.

Figure 10: Comparison between (a) the pore chord and (b) solid chord distribution of a quarried Sebastopol stone, (c) the pore chord and (d) solid chord distribution of a quarried tuffeau.

Figure 11: Comparison between the chord distributions of (a) the moderately weathered zone shown in Figure 1e, (b) the no weathered zone shown in Figure 1f, (c) and (d) the strongly weathered zones shown in Figure 1c and d.

	Number of images	Average porosity (%)	Standard deviation (%)
Quarried tuffeau	8	30.5	2.5
Quarried sebastopol stone	7	35.6	2.4
Weathered tuffeau			
Strongly weathered zone	7	45.2	2.1
Moderately weathered zone	7	28.6	2.3

Table 1: Average total porosity and standard deviation recorded for the stone samples studied.

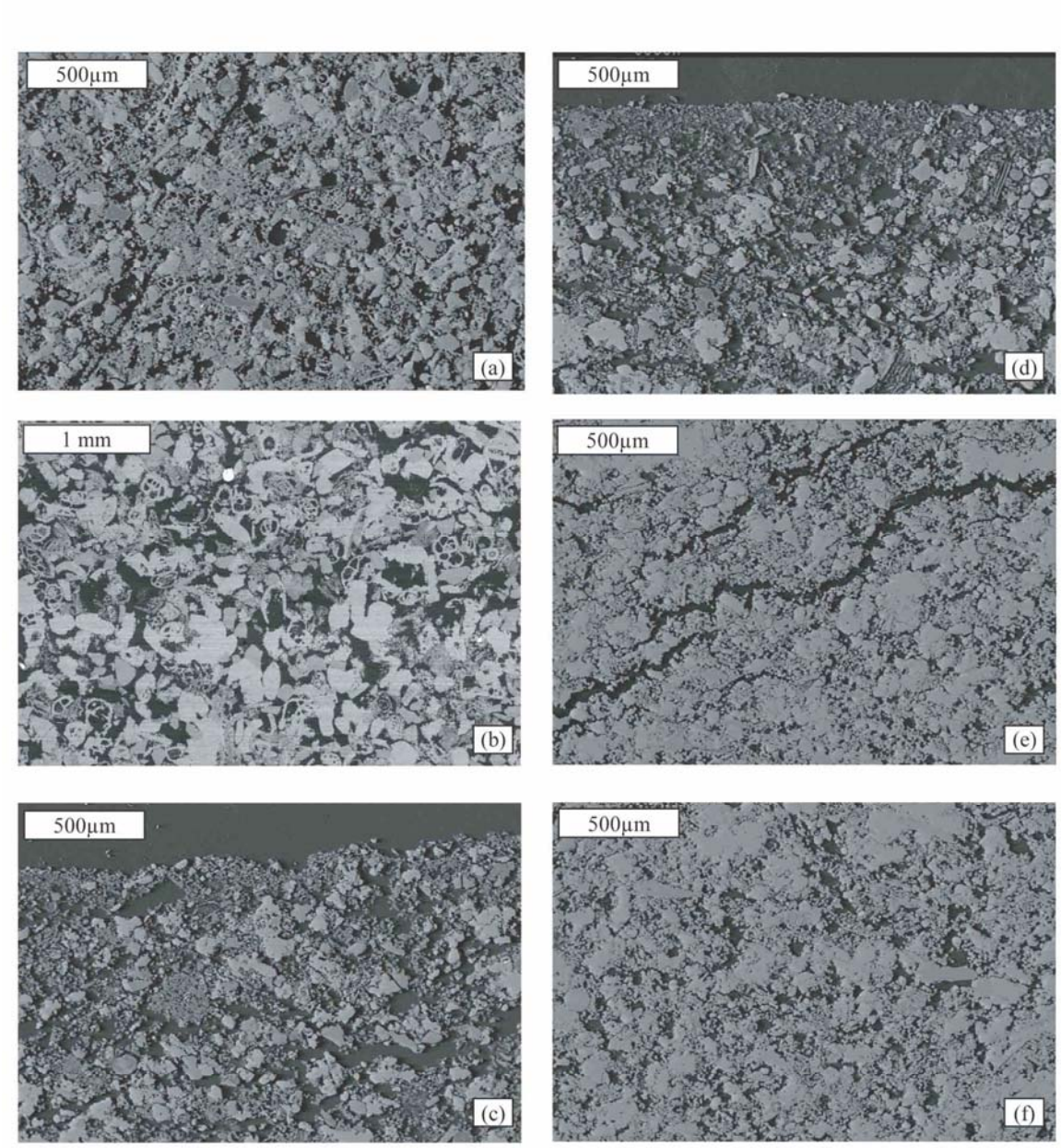

Figure 1

Rozenbaum *et al.*

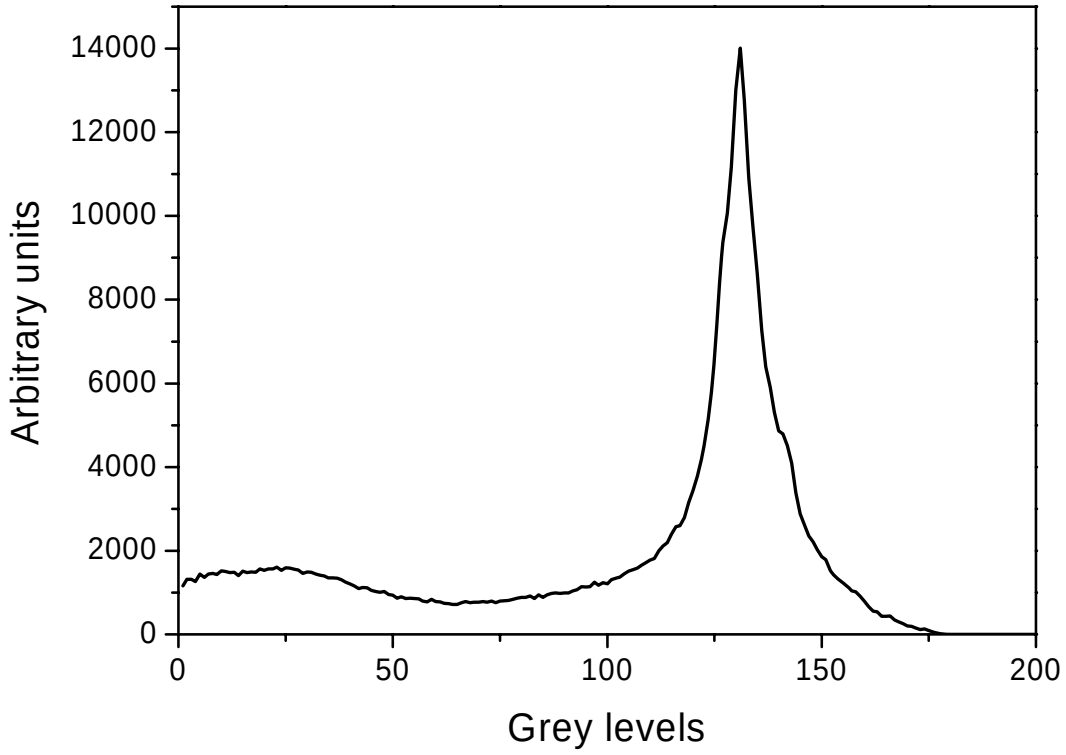

Figure 2

Rozenbaum *et al.*

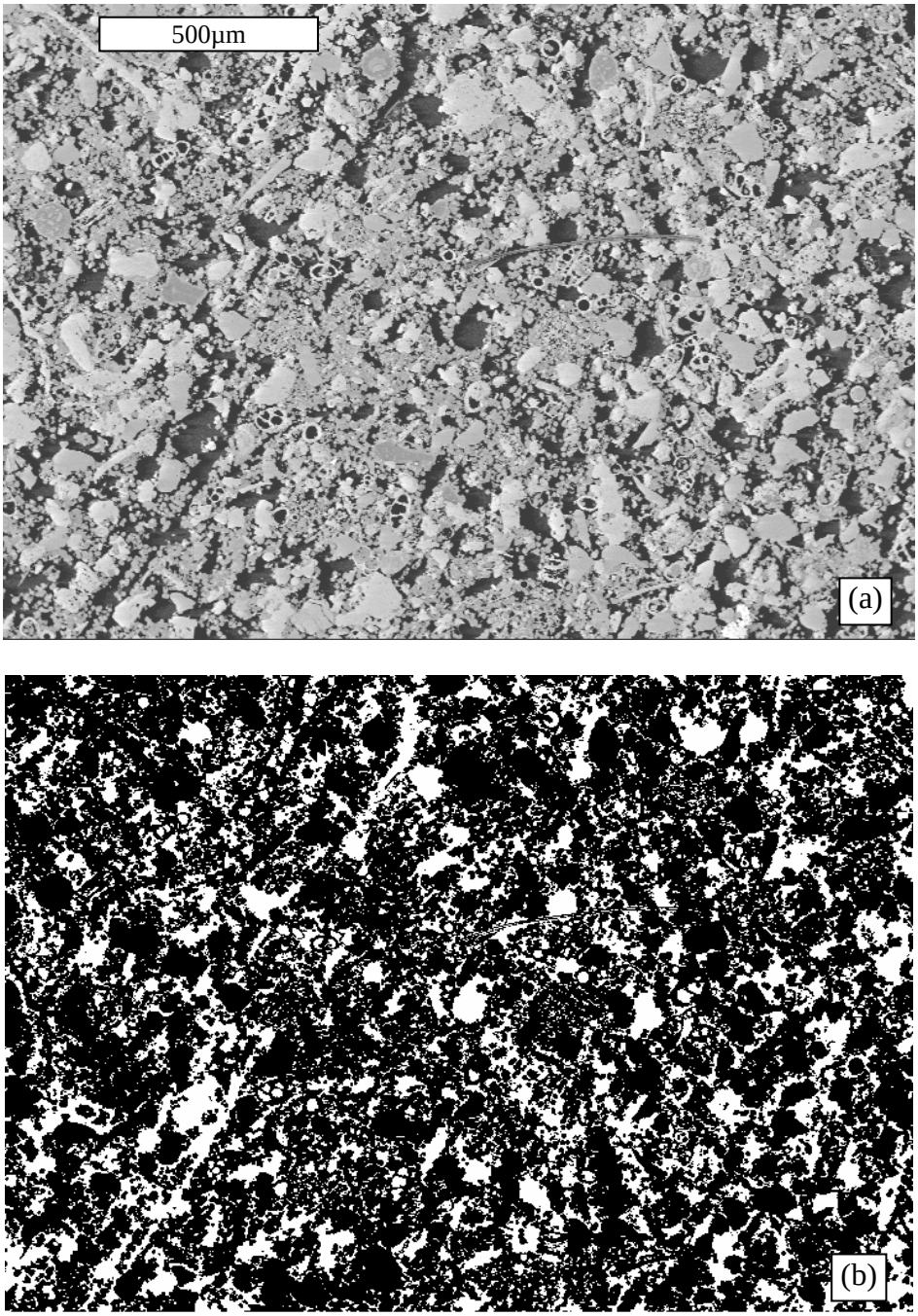

Figure 3

Rozenbaum *et al.*

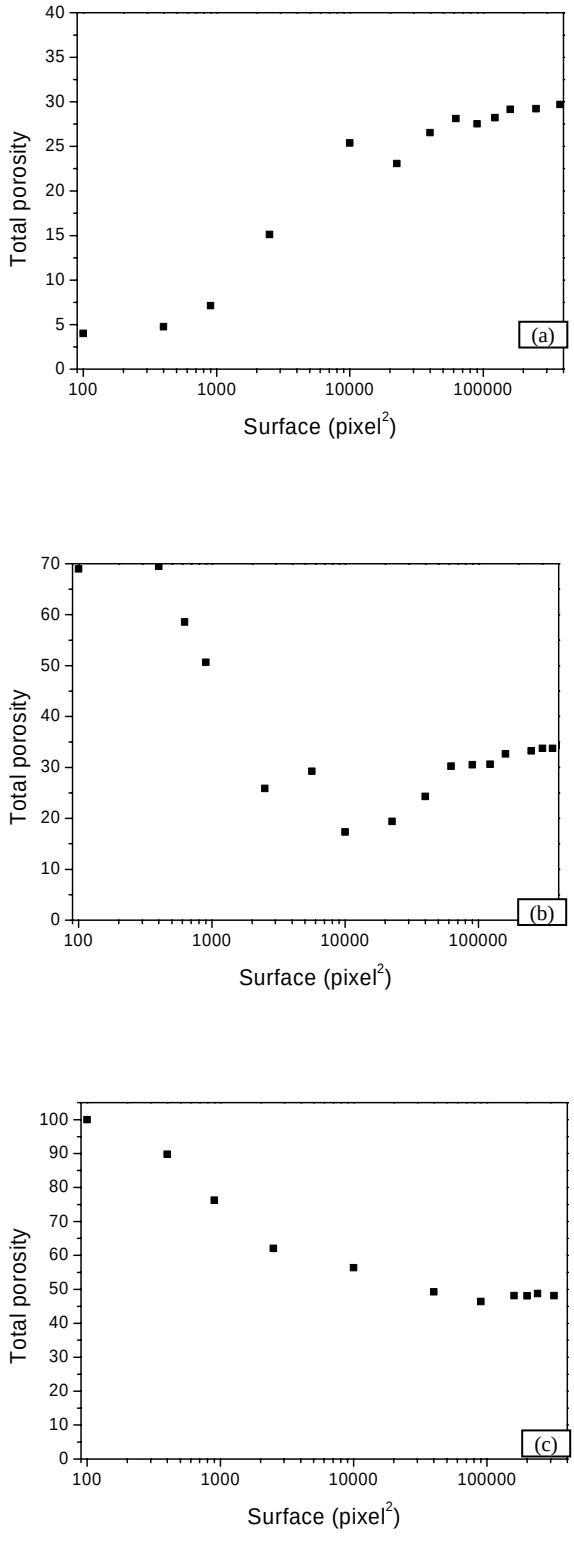

Figure 4

Rozenbaum *et al.*

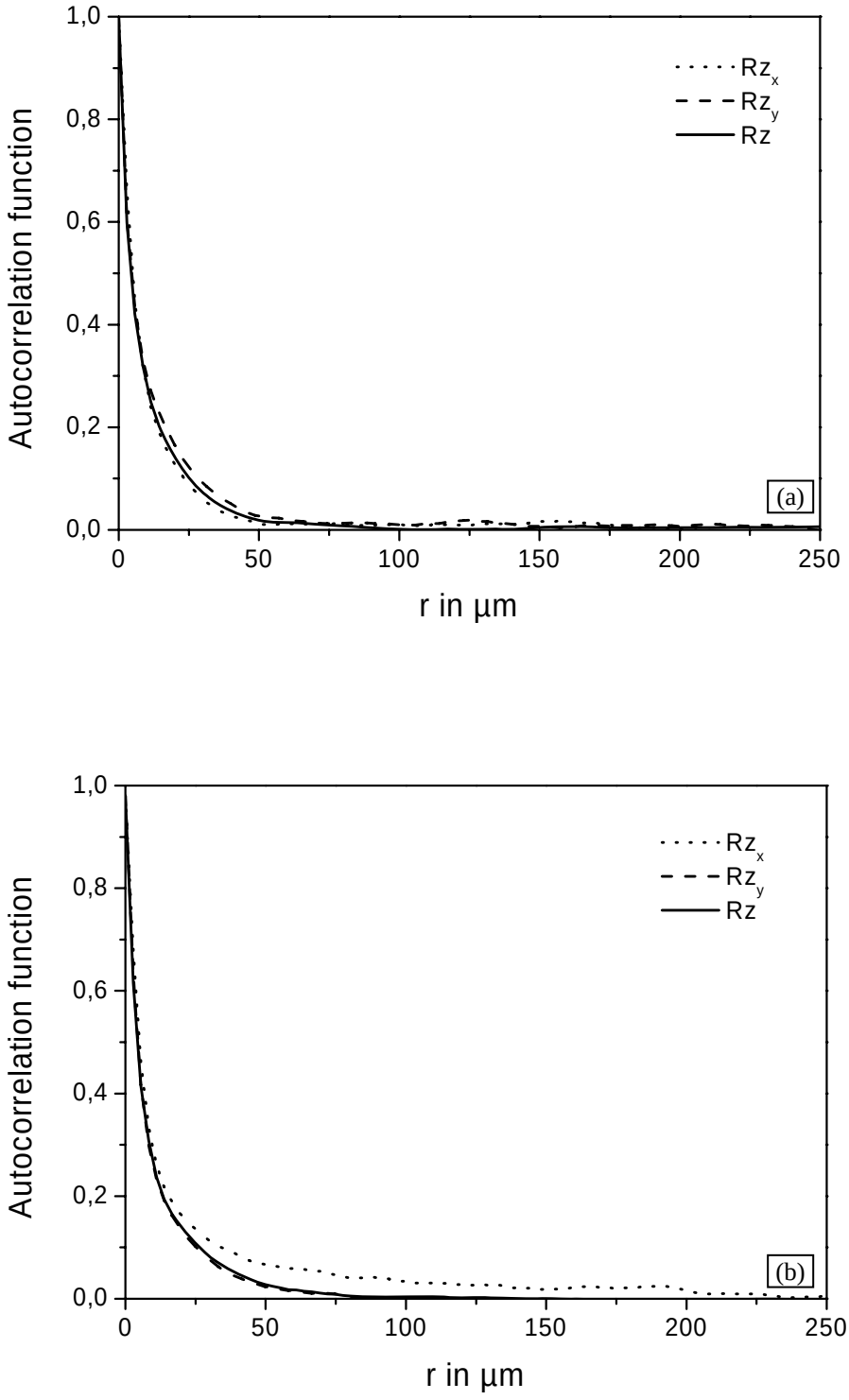

Figure 5

Rozenbaum *et al.*

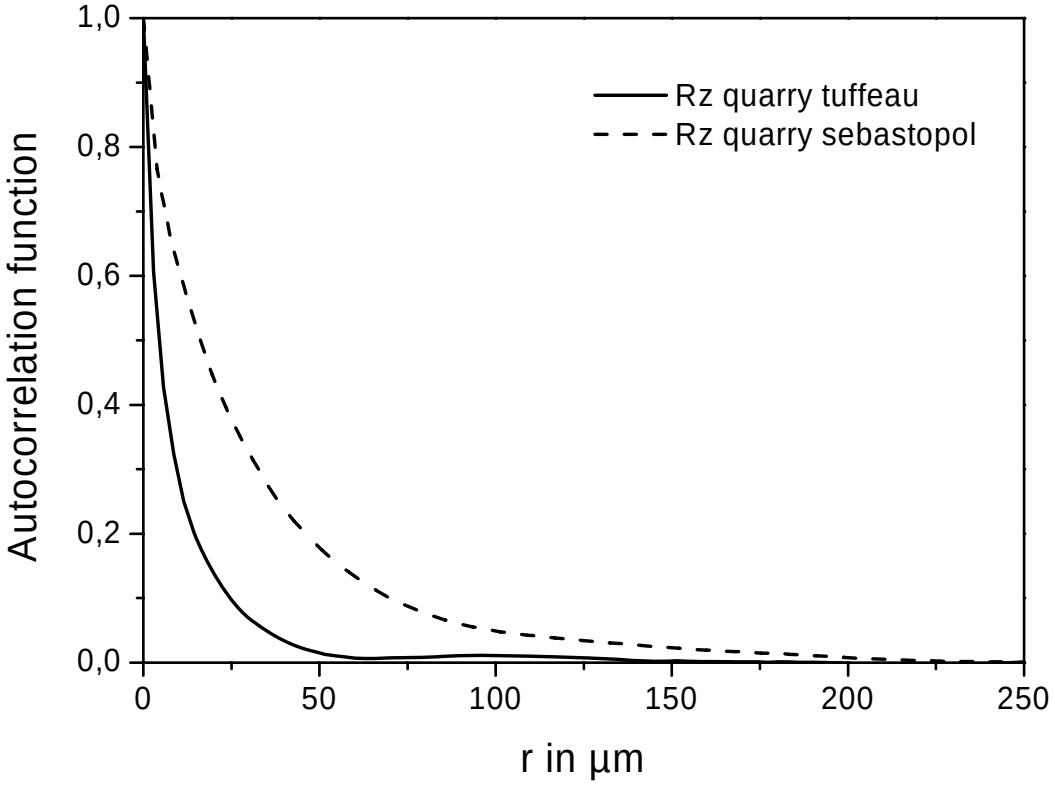

Figure 6

Rozenbaum *et al.*

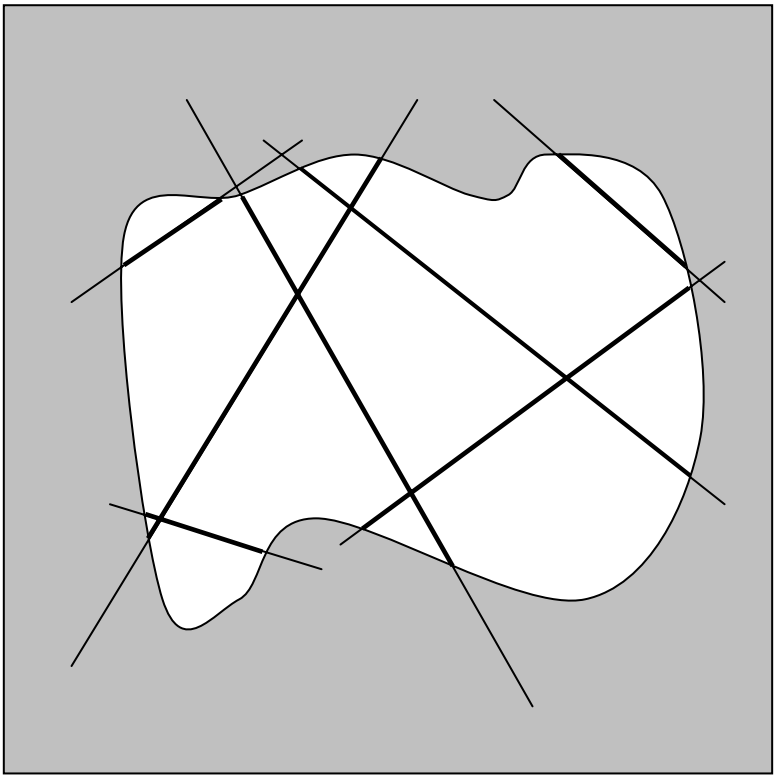

Figure 7

Rozenbaum *et al.*

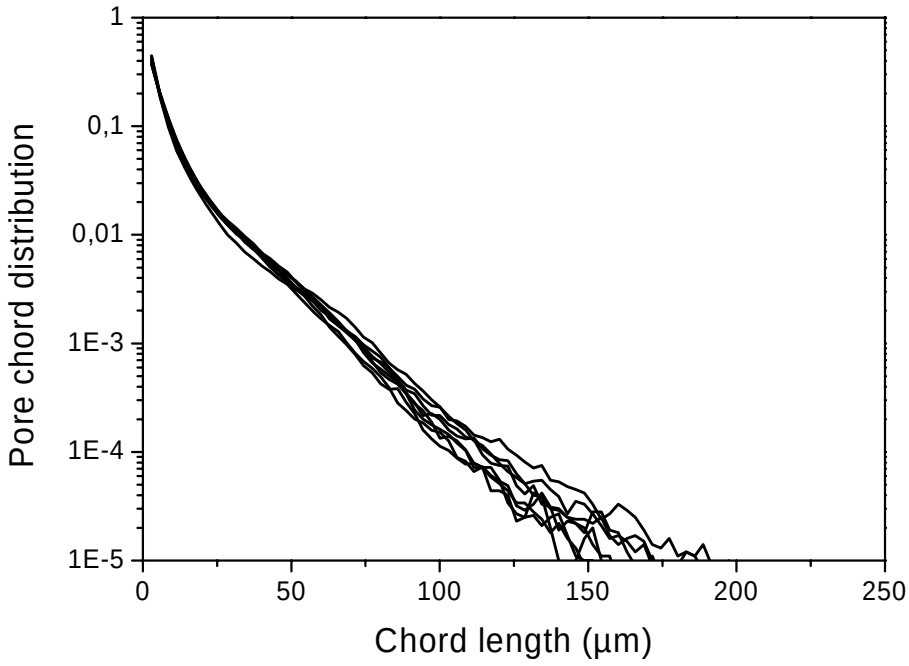

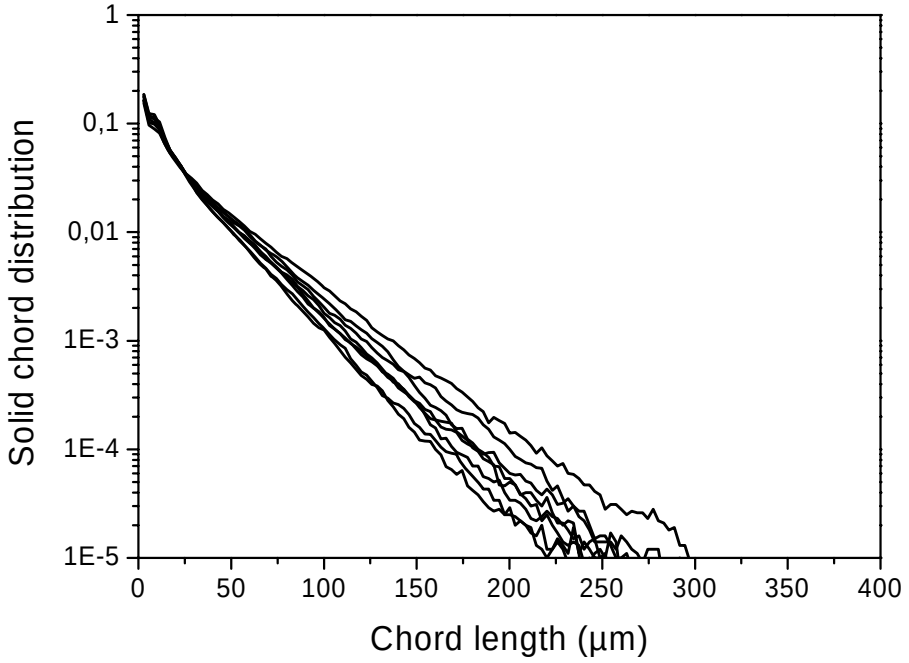

Figure 8

Rozenbaum *et al.*

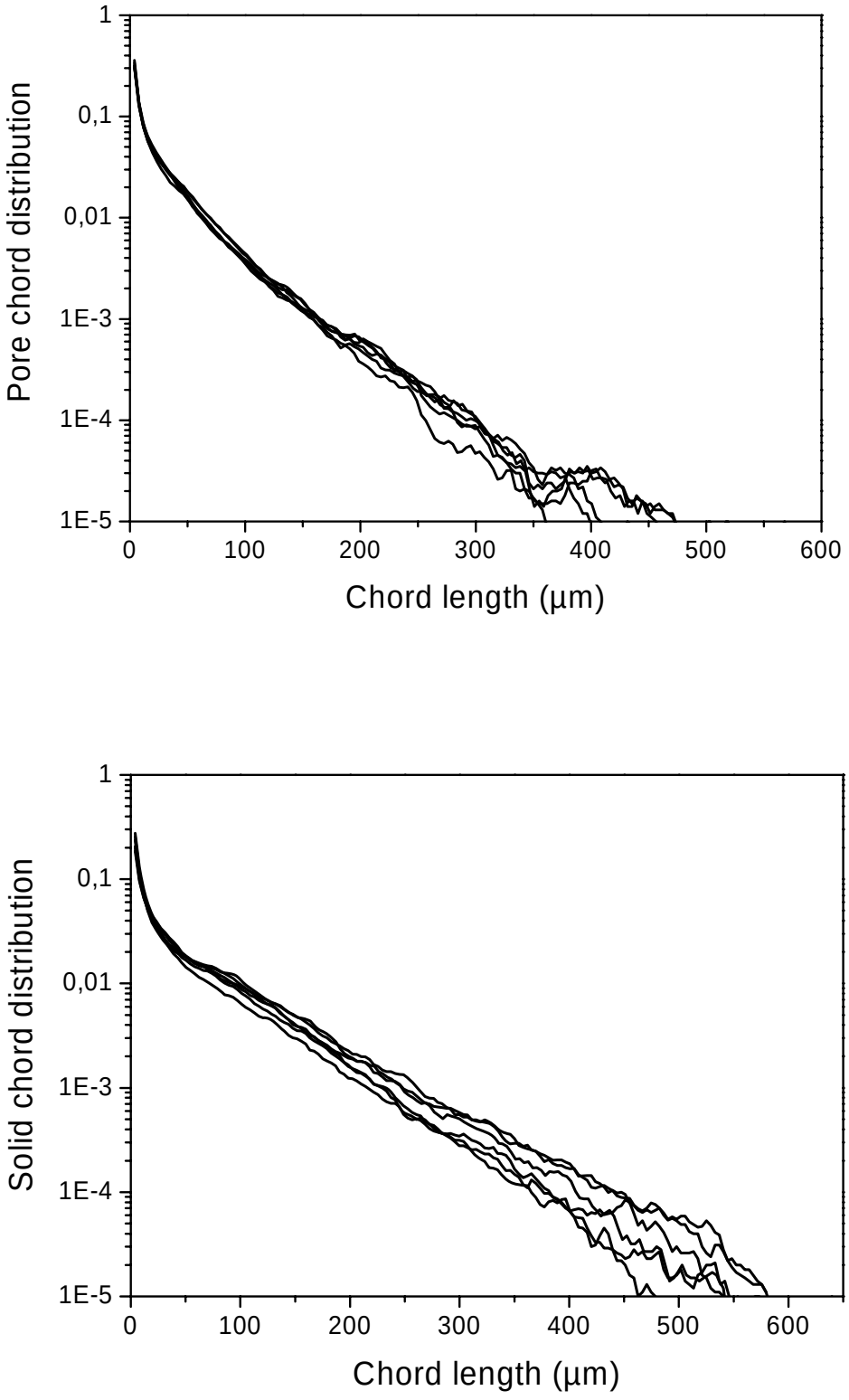

Figure 9

Rozenbaum *et al.*

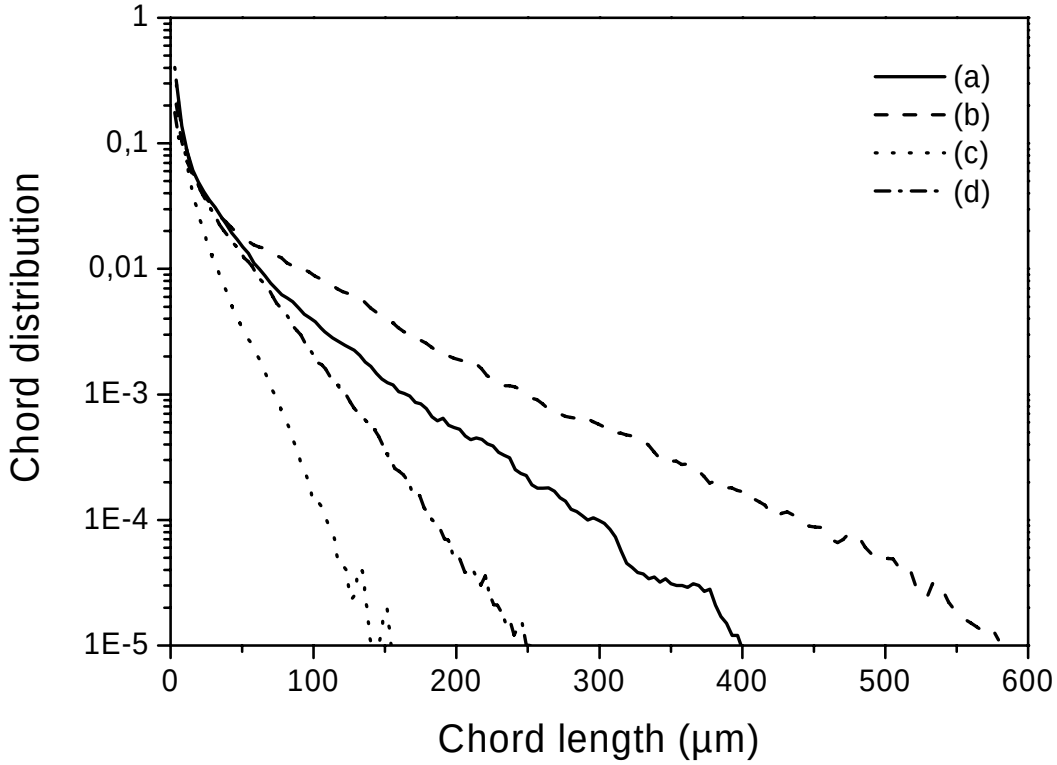

Figure 10

Rozenbaum *et al.*

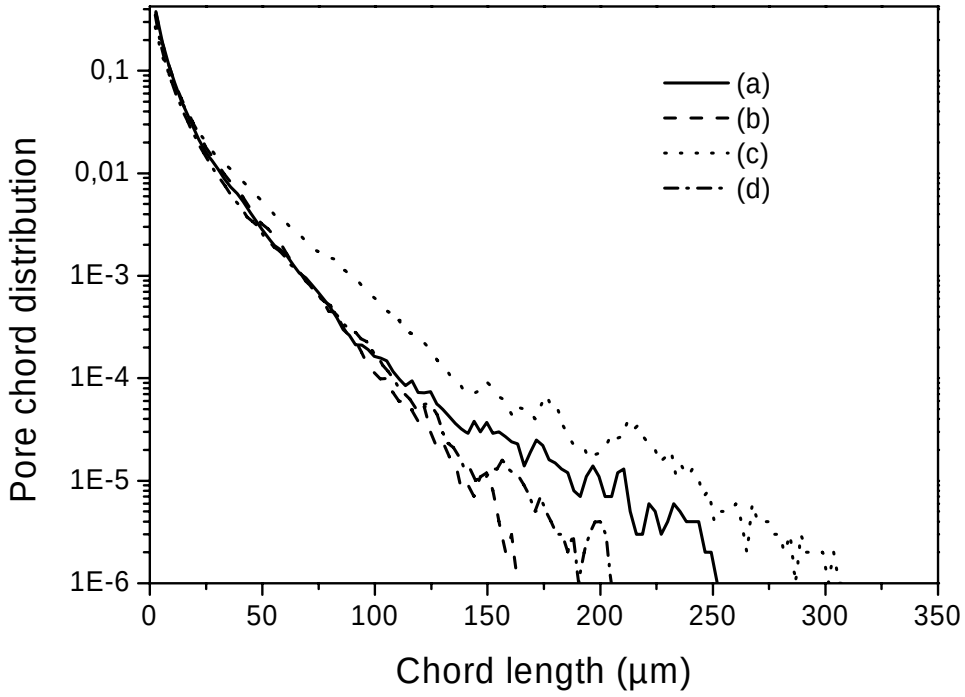

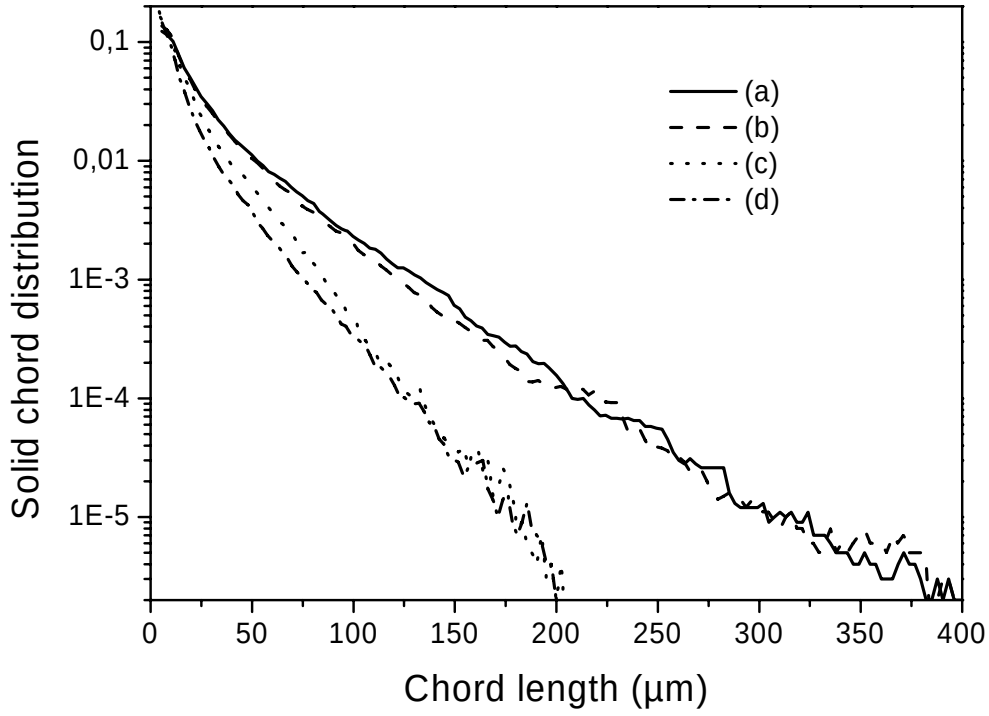

Figure 11

Rozenbaum *et al.*